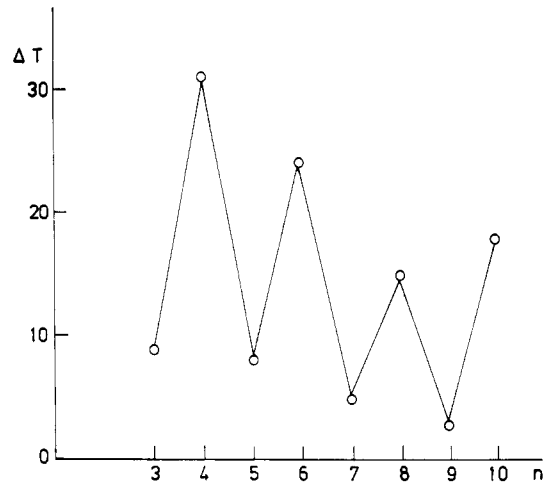

Figure 6. Plot of supercooling effect ($\Delta T = T_i - T_i$) against spacer length.

that the mesomorphic order can be locked into the glassy state by quenching rapidly from the isotropic phase. Such pretransitional order induced by this mechanical shock might be one of the contributing factors to this unusual effect on making the isotropic to the mesomorphic transition.

Acknowledgment. We thank SERC for financial support for H.H.W., enabling us to undertake this work.

Registry No. I, 15552-32-6; II, 57045-26-8; III, 106610-62-2; (IV)(ClCO(CH_2)$_3$COCl) (copolymer), 115339-58-7; (IV)(ClCO(CH_2)$_3$COCl) (SRU), 115339-51-0; (IV)(ClCO(CH_2)$_4$COCl) (copolymer), 106608-01-9; (IV)(ClCO(CH_2)$_4$COCl) (SRU), 106707-10-2; (IV)(ClCO(CH_2)$_5$COCl) (copolymer), 115339-59-8; (IV)(ClCO(CH_2)$_5$COCl) (SRU), 115339-52-1; (IV)(ClCO(CH_2)$_6$COCl) (copolymer), 115339-60-1; (IV)(ClCO(CH_2)$_6$COCl) (SRU), 115339-53-2; (IV)(ClCO(CH_2)$_7$COCl) (copolymer), 115339-61-2; (IV)(ClCO(CH_2)$_7$COCl) (SRU), 115339-54-3; (IV)(ClCO(CH_2)$_8$COCl) (copolymer), 115339-62-3; (IV)(ClCO(CH_2)$_8$COCl) (SRU), 115339-55-4; (IV)(ClCO(CH_2)$_9$COCl) (copolymer), 115339-63-4; (IV)(ClCO(CH_2)$_9$COCl) (SRU), 115339-56-5; (IV)(ClCO(CH_2)$_{10}$COCl) (copolymer), 115339-64-5; (IV)(ClCO(CH_2)$_{10}$COCl) (SRU), 115339-57-6; (COHB)(MAA) (copolymer), 115339-65-6; ethyl chloroformate, 541-41-3; *p*-hydroxybenzoic acid, 99-96-7; *cis*-1,5-cyclooctanediol, 23418-82-8.

References and Notes

(1) Lehmann, O. *Z. Phys. Chem., Stoechiom. Verwandtschaftsl.* **1889**, *4*, 462.
(2) Friedel, A. *Ann. Phys.* (Leipzig) **1922**, *18*, 273.
(3) Dobb, M. G.; McIntyre, J. E. *Adv. Polym. Sci.* **1984**, *60/61*, 61.
(4) Ober, C. K.; Jin, J. I.; Lenz, R. W. *Adv. Polym. Sci.* **1984**, *59*, 103.
(5) De Gennes, P. G. *C. R. Seances Acad. Sci., Ser. B* **1975**, *B281*, 101.
(6) Cowie, J. M. G.; Wu, H. H. *Polym. Bull. (Berlin)* **1986**, *16*, 327.
(7) Cowie, J. M. G.; Wu, H. H. *Liq. Cryst.*, in press.
(8) Gray, G. W.; Goodby, J. W. G. *Smectic Liquid Crystals*; Leonard Hill: London, 1984.
(9) Asrar, J.; Toriumi, H.; Watanabe, J.; Krigbaum, W. R.; Ciferri, A.; Preston, J. *J. Polym. Sci., Polym. Phys. Ed.* **1983**, *21*, 1119.
(10) Meurisse, P.; Noel, C.; Monnerie, L.; Fayolle, B. *Br. Polym. J.* **1981**, *13*, 55.
(11) Roviello, A.; Sirigu, A. *J. Polym. Sci., Polym. Lett. Ed.* **1975**, *13*, 455.
(12) Griffin, A. C.; Havens, S. J. *J. Polym. Sci., Polym. Lett. Ed.* **1980**, *18*, 259.
(13) Braun, D.; Schulke, U. *Makromol. Chem.* **1986**, *187*, 1145.
(14) Roviello, A.; Sirigu, A. *Makromol. Chem.* **1982**, *183*, 895.
(15) Strzelecki, L.; Liebert, L. *Eur. Polym. J.* **1980**, *16*, 303.
(16) Ober, C.; Jin, J. I.; Lenz, R. W. *Polym. J. (Tokyo)* **1982**, *14*, 9.
(17) Marzotko, D.; Demus, D. *Liq. Cryst., Proc. Int. Conf.* **1975**, *1*, 189.
(18) Blumstein, A.; Thomas, D. *Macromolecules* **1982**, *15*, 1264.
(19) Watanabe, J.; Krigbaum, W. R. *Macromolecules* **1984**, *17*, 2288.

A New Theory of Entanglements and Dynamics in Dense Polymer Systems

Tom A. Kavassalis* and Jaan Noolandi*

Xerox Research Centre of Canada, 2660 Speakman Drive, Mississauga, Ontario L5K 2L1, Canada. *Received November 6, 1987; Revised Manuscript Received January 29, 1988*

ABSTRACT: The entanglement concept, which is central to the reptation theory, has been reformulated. The phenomenological parameter, N_e, introduced by de Gennes and Doi and Edwards, has been replaced by a new parameter, $\tilde{N}$, called the coordination number, which can be computed from the conformational statistics of many chains, in a melt or concentrated solution. It is argued that, with the appropriate choice of $\tilde{N}$, one can relate this quantity to the mean entanglement spacing according to a simple relation. $\tilde{N}$, which is a preaveraged topological parameter, also provides a criterion for the presence of entanglements and describes the degree of entanglement in terms of the chain parameters and polymer density. The mean entanglement spacing is shown to depend on the degree of polymerization in the region of the transition. The transition from entangled to unentangled behavior, which is geometrical in origin, follows from this theory as do several well-established scaling laws for melts and concentrated solutions. A generalized Rouse model (GRM), modified to incorporate entanglement effects, has been used with this theory to describe polymer dynamics in entangled and unentangled melts. The reptation theory results are recovered in the asymptotic long-chain limit.

1. Introduction

Recently, the mechanical and transport properties of polymer melts and concentrated solutions have been of considerable experimental and theoretical interest.[1] Despite the chemical and structural diversity of linear polymeric systems, most exhibit universal behavior in their rheological properties that is depicted in Figure 1. For low molecular weight melts, the zero shear viscosity, η_0, is proportional to the degree of polymerization, N, whereas for high molecular weights, the zero shear viscosity scales as some higher power of N, typically $N^{3.4}$. The transition occurs at a degree of polymerization, N_c, which varies from one polymer to the next. It is now well-known that this change in the scaling law can be attributed to the formation of entanglements amongst chains in the high molecular weight regime.

Most theories, for the dynamics in these systems, are of the mean field type in that they focus on the motion

0024-9297/88/2221-2869$01.50/0

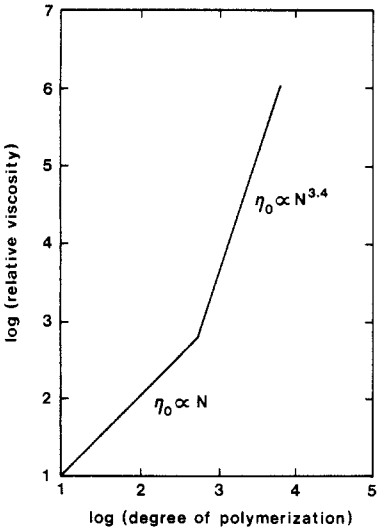

Figure 1. Schematic plot of zero shear rate viscosity, η_0, versus degree of polymerization, N, for a melt of linear polymers. Low molecular weight melts exhibit the $\eta_0 \propto N$ scaling law in agreement with the Rouse theory for unentangled polymers. High molecular weight melts typically exhibit the $\eta_0 \propto N^{3+\delta}$ scaling law where δ is usually in the range of $\sim$0.4. The change in scaling law is due to the high degree of entanglement that exists in these systems. The reptation theory[2,3] qualitatively describes the rheology of entangled systems but predicts $\delta = 0$.

of a single chain in a concentrated environment of other chains. The reptation or tube model of de Gennes[2] and Doi and Edwards[3] has been very successful in qualitatively describing the dynamics of polymeric melts in the entangled regime. In the reptation model, a polymer diffuses in a dense network of entanglements formed by the surrounding chains. The model assumes that the entanglements are sufficiently long-lived so that the diffusional motion is essentially one-dimensional in a confining tube. The flow properties are then determined by the time required for each chain to wriggle out of its confining tube into a new configuration.

In the reptation theory, the detailed conformation of the polymer chain is replaced by a connected sequence of freely jointed beads or links corresponding to equal-sized segments of polymer. The number of skeletal bonds per link is equal to the mean spacing between entanglements, N_e. The conformation of the polymer segment between the entanglement points is assumed to change rapidly compared to the overall chain conformation, and thus the chain can be represented by a coarse grained image of jointed beads that evolves along a primitive path, defined by the entanglement points. It is in this sense that the polymer is thought of as being confined to a tube that is stochastically created and destroyed at the ends.

The tube renewal time can then be computed by assuming that the mobility of the chain in the tube is inversely proportional to the number of chain segments N

$$\mu_{tube} = \mu_0/N \tag{1}$$

where μ_0 is the mobility per tube segment. The diffusion constant for the curvilinear motion of the polymer in the tube is given by the usual Einstein relation

$$D_{tube} = \mu_{tube} k_B T \propto N^{-1} \tag{2}$$

The tube renewal time, τ_r, then follows according to

$$\tau_r = L^2/D_{tube} \propto N^3 \tag{3}$$

where $L \propto N$ is the length of the tube. The self-diffusion coefficient can be obtained by similar arguments

$$D_{self} = R_g^2/\tau_r \propto N^{-2} \tag{4}$$

where $R_g \propto N^{1/2}$ is the polymer's radius of gyration. Experiments on high molecular weight melts are generally in agreement with the predictions of the reptation theory but yield a slightly higher exponent of 3.4 for the zero shear viscosity, which is proportional to τ_r.

In the reptation theory, the phenomenological parameter, N_e, is assumed to be a property of the entangling chains and independent of the total chain length. While N_e is central to the tube concept, a direct calculation of N_e, for a particular system, has not been accomplished because of the difficulty of topologically classifying entanglements. In practice, N_e is used as an experimental fitting parameter using the plateau modulus, $G_N^0 \propto 1/N_e$, which is directly related to N_e in the tube model. The experimentally determined values of N_e vary from one polymer to the next, and attempts have been made to correlate this variation to the chain parameters.[4]

The dynamics of unentangled polymers are usually described by variations on the traditional Rouse model.[5] Here the polymer is represented by a series of connected beads and springs which are allowed to move randomly in three dimensions under the action of Langevin forces. In the Rouse model, the "springs" obey Gaussian statistics and have a spring constant $k = 3k_BT/b^2$, where b is the equilibrium spring length. The intermolecular interactions are assumed to be dissipative and are represented by a monomer friction coefficient, ζ_0.

The resulting equations of motion for the Rouse model can be solved straightforwardly by constructing the Fourier modes, $\tilde{\mathbf{R}}_p(t)$,[6]

$$\tilde{\mathbf{R}}_p(t) \equiv 2^{1/2} \sum_{n=1}^{N} \mathbf{R}_n(t) \cos(\pi p n/N) \tag{5}$$

where p is an integer $p = 1, 2, 3, ..., N$, $\mathbf{R}_n(t)$ is the position of bead n, and N is the total number of beads in the chain. The relaxation time for the mode with wavenumber p is

$$\tau(p) = \zeta_0/[2k(1 - \cos(\pi p/N))] \tag{6a}$$

$$\tau(p) \propto \zeta_0 N^2/k\pi^2 p^2 \qquad p \ll N \tag{6b}$$

and describes the time scale for the evolution of the section of the chain with N/p beads.

Once the relaxation times are known, several results can be readily obtained from the Rouse model. For example, the self-diffusion coefficient and zero frequency shear viscosity are[6]

$$D_G = k_BT/N\zeta_0 \tag{7}$$

$$\eta_0 = c\zeta_0 N k^2/36 \tag{8}$$

respectively, where c is the concentration.

Recently, several new theoretical and computational approaches to polymer dynamics have been developed. Hess,[7] for example, starts with a Fokker–Planck equation for the phase space distribution function for all polymer segments and invokes a projection operator to derive a formal expression for the diffusion coefficient similar to the Green–Kubo formulae.[8,9] The formalism incorporates scaling theory results, which lack numerical coefficients, and consequently Hess invokes a phenomenological entanglement parameter, N_c. Kolinski et al.[10] have employed dynamic Monte Carlo methods to study the nature of dense melt dynamics and reported no evidence for a tube or reptational motion. Their results however do not eliminate reptation as the dominant mechanism at higher densities and for very long chains.

In this paper, we introduce a reformulation of the tube ansatz. The phenomenological parameter, N_e, is replaced by a new parameter, $\tilde{N}$, called the coordination number,

whose value is determined from the statistical properties of many chains in a melt or solution. In the present theory, $\tilde{N}$ is a geometrical property of the entangling chains and is related to N_e and N_c, the critical chain length for the presence of long-lived entanglements. The value of N_e that we predict is not independent of the total chain length but becomes independent as the chains become longer. It also depends on chain properties such as the characteristic ratio and the monomer composition as well as the polymer melt density.

For polymer melts and concentrated ideal solutions, the dynamics in the entangled state can then be described by a suitable projection of the Rouse equations onto a tube axis. The tube axis is defined as a Fourier smoothened image of the chain which evolves according to a generalized Rouse model (GRM) that is modified to incorporate the influence of entanglements.

In section 2, we present our model for entanglements in dense polymer systems and discuss various scaling predictions of the theory. In section 3 we review the basic elements of the GRM and discuss its application to polymer melts. In section 4, we apply our model of entanglements and the GRM to compute the relaxation spectrum for entangled and unentangled polymer systems and discuss the viscosity and diffusion coefficients.

2. Entanglement Theory

In this section, we propose a quantitative description of entanglements, or more simply lateral constraints, that is based on a static mean field description of the environment surrounding a test chain. Our system of interest consists of a melt of Gaussian monodisperse chains with degree of polymerization N, bond length l, and bond number density ρ_m. The characteristic ratio, C_∞, of the chains is taken to be unity, and we will simply quote results for systems with $C_\infty \neq 1$. We will use the terms monomer and bond interchangebly for this system. For the remainder of this article, we will use the symbol N and the term degree of polymerization to refer to the number of skeletal bonds in a polymer chain. The bond length, l, is then the appropriate average bond length.

Focusing on one chain, hereafter called the test chain, we inscribe a subsection of the chain in a sphere with diameter $D_e = N_e^{1/2}l$, i.e., the mean distance spanned by the N_e bonds (see Figure 2). For the moment, N_e will be some arbitrary number less than N. In a high-density system, several other polymers will thread through this sphere and may be involved in forming entanglements with the test chain segment or may restrict the lateral degrees of freedom of the chain. With the help of Figure 2, we can see that the probability of this situation occurring is not independent of chain lengths. For example, if we rescale all polymer lengths according to $N \rightarrow N/2$ by simply cutting all polymers at their midpoints (Figure 2 lower panel), some of our scissions will occur within the test sphere. The new polymer ends produced by this cutting will lessen the probability of having entanglements or lateral constraints within the original sphere and increase the mean spacing between entanglements accordingly.

We can quantify these arguments as follows. Let $N(m)$ be the mean number of other polymer segments with exactly m bonds within the test sphere. By mean number, we refer to an average over all possible conformations of the surrounding chains. Ascribing a volume l^3 to each bond, we can relate the volume of the sphere, V_e, to $N(m)$ by using

$$\phi V_e = l^3(N_e + \sum_{m=1}^{N} N(m)m) \tag{9}$$

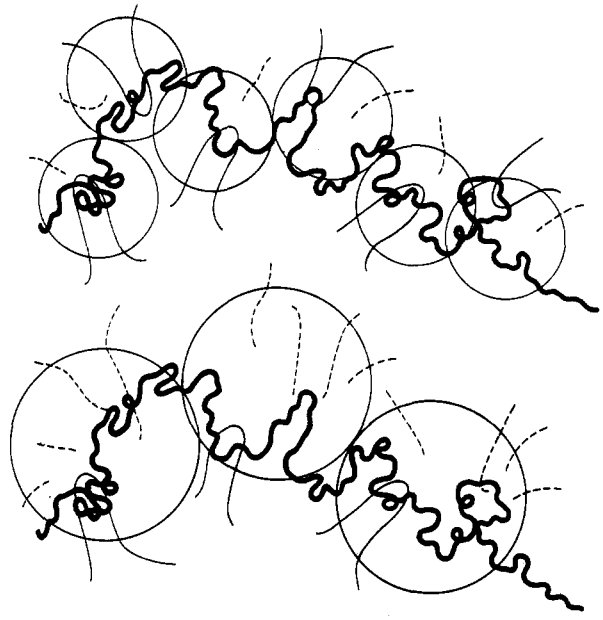

Figure 2. Schematic illustration of the entangled state. The heavy solid line represents a portion of the test chain. In each picture, the entangling chains are represented by solid loops surrounding the test chain and enclosed in spheres with diameter $\sim N_e^{1/2}l$. The upper and lower portions of the figure illustrate the effect of polymer length on the spacing between entanglements. In our model, a lateral constraint is related to the number of polymers, $\tilde{N}$ (coordination number), threading through the sphere and surrounding a segment of the test chain. In the upper figure, the test chain is divided into six blobs, as defined by the $6\tilde{N}$ constraining chains. In the lower figure, where the surrounding chains are shorter, the blob volume is enlarged to enclose the same number of constraining chains per blob. The dotted lines in the figure represent tail segments, which are ineffective in constraining the diffusional motion of the chain in our model. The lower figure shows proportionally more tail segments enclosed in the spheres.

where $V_e = \pi N_e^{3/2}l^3/6$ and ϕ here is the polymer volume fraction. The first term on the right-hand side of eq 9 is due to the test segment and the second term is due to all other segments threading through the volume. For more general polymers, that is with bond correlations, side groups, etc., the volume, V_e, should be replaced with $V_e = C_\infty^{3/2}N_e^{3/2}l^3/6$, where C_∞ is the characteristic ratio of the polymer. We will simply absorb the value of C_∞ into ϕ by defining ϕ to be $\phi = \rho_m C_\infty^{3/2}l^3 = \rho C_\infty^{3/2}l^3/\mu_m$, where ρ is the mass density of the melt and μ_m is the monomer mass per skeletal bond.

$N(m)$ is a statistical quantity and can be readily computed by Monte Carlo methods. Several scaling properties of the distribution $N(m)$ can, however, be established from geometrical arguments. For example, for small m, $N(m)$ should increase with the surface area of the test volume. This represents polymers with only a few beads in the volume, and hence they must appear at the surface of the sphere. This property is demonstrated in Figure 3, where $N(m)$ is calculated from random flights ($C_\infty = 1$) generated in spheres with diameter $D_e = 4l$ and $8l$. While $N(m)$ is largest for small m, the small m values make a negligible contribution to the sum in eq 9. The product $N(m)m$, plotted in Figure 4 versus m, shows a broad maximum centered near $D_e^2/2$ with a long tail to the right of the maximum. Most of the weight in $\sum N(m)m$ is derived from the lengths m around $D_e^2/2$.

The statistical distribution of polymer segments can be further classified into two contributions

$$N(m) = N_{\text{tails}}(m) + N_{\text{nontails}}(m) \tag{10}$$

where the two terms represent segments with tails and

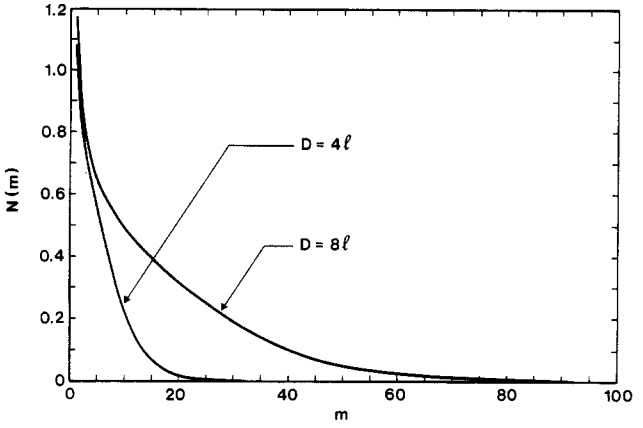

Figure 3. Polymer segment length distribution functions for random flights (N = 500) grown in spherical volumes with diameter $D = 4l$ and $8l$. $N(m)$ is the mean number of segments with exactly m beads in the volume. The statistics were generated by first picking and labeling a reference bead from 1 to N at random. This bead was then randomly placed in the spherical volume, and polymer conformations were grown randomly in both directions (i.e., toward bead 1 and bead N) until either the random walk left the spherical volume or the end of the polymer was reached. The figures were generated by averaging the results of 5×10^6 such walks.

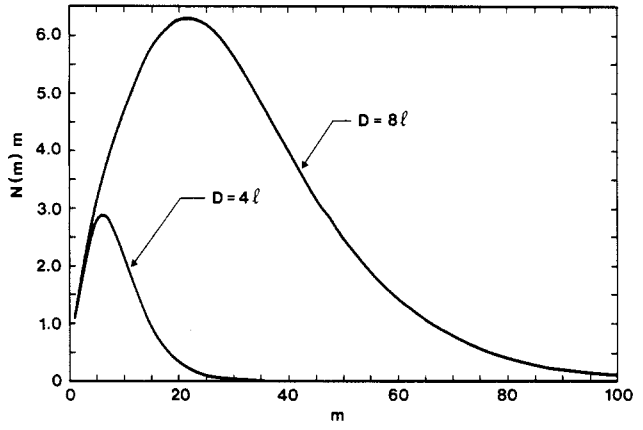

Figure 4. Data from Figure 4 replotted as $N(m)m$ versus m. This statistic represents the distribution of polymer mass found in the spherical volume. The curves show a broad maximum centered at $m \sim D^2/2$, which indicates that the majority of the spherical volume is, on the average, made up of segments of polymer whose length is of the same order as the dimensions of the sphere. These data confirm our physical interpretation of the coordination number, $\tilde{N}$, as discussed in section 2.

without tails and having exactly m bonds in the volume. With the previous definitions, we can rewrite eq 9 as

$$\phi V_e = l^3(N_e + N_e\tilde{N} + \sum_{m=1}^{N} N_{\text{tails}}(m)m) \tag{11}$$

where we have introduced a new parameter, $\tilde{N}$, which we call the coordination number defined as

$$\tilde{N} = N_e^{-1} \sum_{m=1}^{N} N_{\text{nontails}}(m)m \tag{12}$$

The coordination number can be ascribed the following physical interpretation. If all segments, excluding tails, that thread through the test volume have the mean length N_e, then $\tilde{N}$ is the number of such segments in the volume. In this case, we would have $N_{\text{nontails}}(m) = \tilde{N}\delta_{m,N_e}$. In general, however, there are contributions to $\tilde{N}$ from all lengths up to N. Figure 5 illustrates that the nontail segments with lengths $m \ll N_e$ and $m \gg N_e$ make a negligible contribution to the summation in $\tilde{N}$ and the sum is mostly derived from those lengths which are of the order of N_e. We are

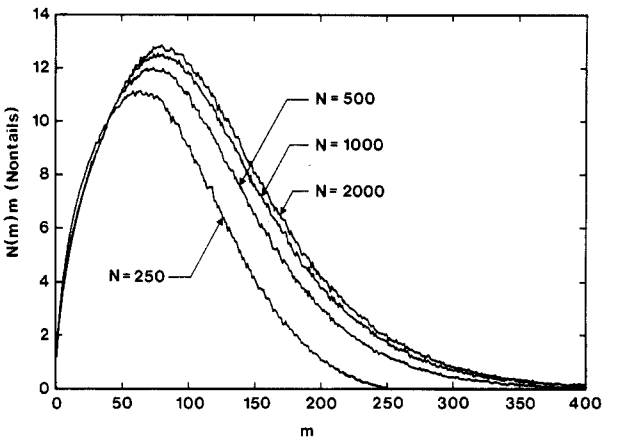

Figure 5. Polymer segment length distributions for random flights grown in a spherical volume with diameter $D = 16l$. $N(m)$ is the mean number of nontail segments with exactly m beads in the volume. The statistics were generated in the same manner as in Figure 3. This figure represents the statistics for walks that did *not* terminate in the sphere. The figure was generated by averaging the results of 5×10^6 walks.

therefore justified in considering $\tilde{N}$ as a measure of the number of nontail polymer segments that thread through the sphere and have length of order N_e.

The tail contribution of eq 11 can be computed as follows. First, we notice that the tail segments are uniformly distributed in the volume. Strictly speaking, we should refer to one end of the polymer as the tail and the other end as the head, and then the tail segments and head segments are separately uniformly distributed, while the separation of the head and tail of a single polymer chain is Gaussianly distributed. The total number of heads and tails (hereafter referred to as tails) is

$$\text{number of tails} = 2\rho_m V_e/N \tag{13}$$

The average tail length, $\langle \text{tail} \rangle$, is therefore

$$\langle \text{tail} \rangle = \sum_{m=1}^{N} N_{\text{tails}}(m)m / \sum_{m=1}^{N} N_{\text{tails}}(m) \tag{14a}$$

$$\langle \text{tail} \rangle = \sum_{m=1}^{N} N_{\text{tails}}(m)m / (2\rho_m V_e/N) \tag{14b}$$

Since the tail segments are uniformly distributed, apart from the Gaussian correlations between the head and tail of a single chain, we have the approximate relation

$$\langle \text{tail} \rangle \approx N_e/2 \tag{15}$$

and therefore

$$\sum_{m=1}^{N} N_{\text{tails}}(m)m \approx \rho_m V_e N_e/N \tag{16}$$

In Figure 6, we plot the distribution of tail lengths, derived from Monte Carlo simulations, to demonstrate that the average tail length is independent of the total chain length in agreement with eq 15.

The average tail length was extracted from the Monte Carlo simulations and is plotted versus the sphere radius in Figure 7. The scaling relation with radius was found to be $\langle \text{tail} \rangle \sim 1.8R^{1.8}$ which corresponds to $\langle \text{tail} \rangle \sim N_e^{0.9}/1.9$ and compares well with the approximate relation in eq 15. The approximation in eq 16 becomes exact in the large N/N_e limit.

Combining eq 14 and 16, we can rearrange eq 11 to write

$$\tilde{N} + 1 = \pi\phi N_e^{1/2}(1 - N_e/N)/6 \tag{17}$$

which relates the coordination number, $\tilde{N}$, to the dimensions of the sphere, the parameter ϕ, and the total chain length.

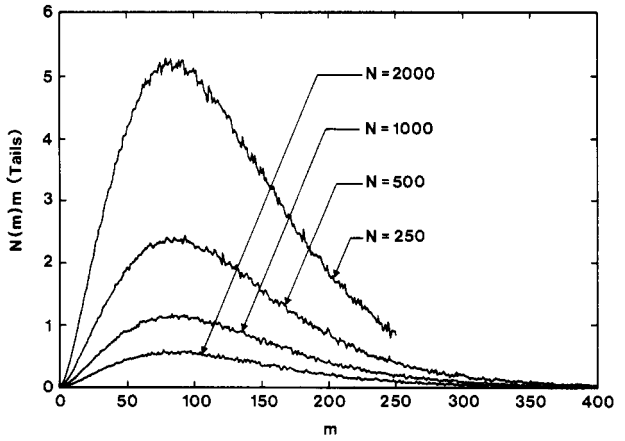

Figure 6. Length statistics for the tail segments. See Figure 5 for details of simulation.

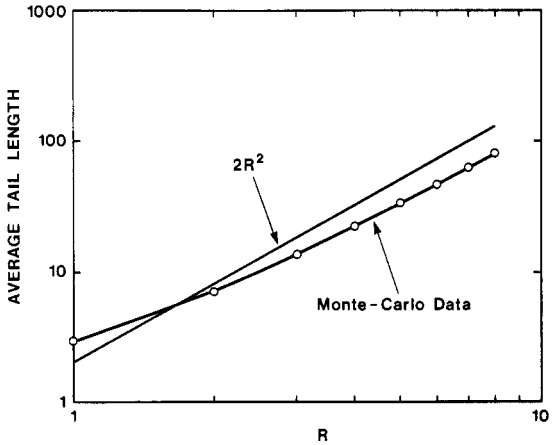

Figure 7. Average tail length versus "blob" radius. The data were extracted from random flight simulations for a fixed polymer length of $N = 1000$. The best fit line to the data was $\langle \text{tail} \rangle = 1.8R^{1.8}$, which compares well to the scaling prediction $\langle \text{tail} \rangle = 2R^2$.

Equation 17 applies to a melt or ideal solution of monodisperse polymer. The preceding analysis can be generalized to polydisperse systems as well. Assuming that we have a distribution of polymer lengths in the system, we then obtain

$$\tilde{N} + 1 = \pi\phi N_e^{1/2}(1 - N_e/\bar{N}_n)/6 \quad (18a)$$

$$\tilde{N} + 1 = \pi\phi N_e^{1/2}(1 - N_e P/\bar{N}_w)/6 \quad (18b)$$

where $\bar{N}_n$ is the number-averaged degree of polymerization, $\bar{N}_w$ is the weight-averaged degree of polymerization, and $P = \bar{N}_w/\bar{N}_n$ is the standard measure of polydispersity. For a two-component blend of chains with length N_1 and N_2 and volume fractions ϕ_1 and ϕ_2, respectively, eq 18 becomes

$$\tilde{N} + 1 = \pi\phi N_e^{1/2}[1 - N_e(\phi_1/N_1 + \phi_2/N_2)]/6 \quad (19)$$

Up to the present, N_e has been an arbitrary length less than N. We now make an ansatz connecting N_e with the mean spacing between entanglements or lateral constraints, by imposing a value for $\tilde{N}$. We will choose $\tilde{N}$ so that, on the average, this number of neighboring nontail segments will constrain the lateral motion of the test segment. These $\tilde{N}$ segments can either be geometrical constraints or complicated knot-like entities, but their precise nature need not be specified. Once $\tilde{N}$ is specified, then N_e can be computed, as a function of N, from eq 17 and interpreted in terms of the mean spacing between constraints. $\tilde{N}$ is a preaveraged topological parameter whose value is expected to be universal and derivable from computer simulations. Specific chain parameters enter

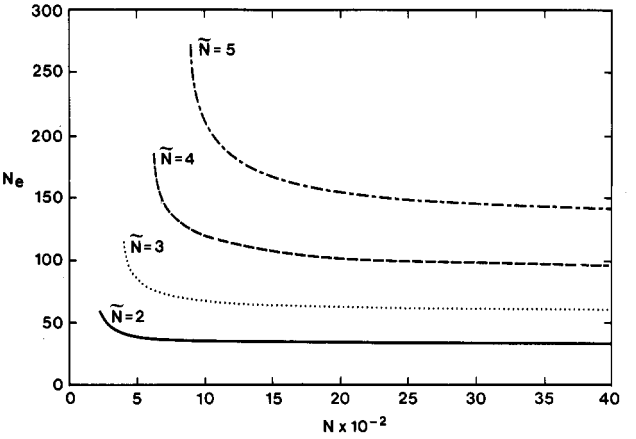

Figure 8. Mean spacing between entanglements versus degree of polymerization for several values of the coordination number $\tilde{N}$ and $\phi = 1$. The curves approach a constant value of $[6(\tilde{N} + 1)/\pi\phi]^2$ for large N. Each curve terminates abruptly at a lower critical chain length, $N_c = 3^5(\tilde{N} + 1)^2/(\pi\phi)^2$. The transition to the unentangled state is geometrical in origin and is due to the increase in polymer tail density and the ineffectiveness of tail segments in forming long-lived constraints.

through the value of ϕ. Therefore, in the present model, N_e is determined by the polymer properties and is not a free parameter.

Several results are readily obtained from eq 17 for monodisperse systems or eq 18 for polydisperse systems. For example, N_e approaches a constant value in the infinite molecular weight limit

$$\lim_{N\to\infty} N_e = [6(\tilde{N} + 1)/\pi\phi]^2 \quad (20)$$

Substituting in the definition of ϕ, we obtain

$$\lim_{N\to\infty} N_e = [6(\tilde{N} + 1)\mu_m/\pi\rho C_\infty^{3/2} l^3]^2 \quad (21)$$

which relates N_e to the various chain parameters and the mass density of polymer.

For any finite value of N, it follows from eq 17 that N_e is larger than the asymptotic limit. In Figure 8 we plot values of N_e versus N, for a monodisperse system, for several choices of the coordination parameter $\tilde{N}$ and $\phi = 1$. Each curve terminates a critical chain length, N_c, below which the number of neighboring nontail segments is less than $\tilde{N}$. All the curves in Figure 8 show a fairly rapid variation of N_e with N just above their respective values of N_c. For larger N, N_e shows a much weaker N dependence and the curves approach their respective asymptotic values of $N_e(\infty)$ given by eq 20. This behavior is contrasted with the Doi–Edwards and de Gennes theories where N_e is taken to be a constant with respect to total chain length, N.

Figure 8 also applies to a polydisperse system with the substitution of $\bar{N}_n$ for N. Here again, the value of N_e varies considerably over a range of more than 1 decade of values of $\bar{N}_n$. Figure 8 can also be applied to a system with constant polydispersity index P, with the substitution of $\bar{N}_w/P$ for N. If, however, the polydispersity index varies with $\bar{N}_w$, as is the case in most experimental situations, the range over which N_e varies with $\bar{N}_w$ will be affected. For example, if P increases slowly with $\bar{N}_w$, e.g., $P \propto \bar{N}_w^{0.1}$, then a plot of N_e versus $\bar{N}_w$ will show a variation of N_e over approximately 2 decades of $\bar{N}_w$ values. This situation is depicted in Figure 9. Note here that the range of variation of N_e depends on which measure of chain length is used to describe the polymer. This will have important consequences as discussed in a later section. For the remainder of this article, we will refer to N_c as the num-

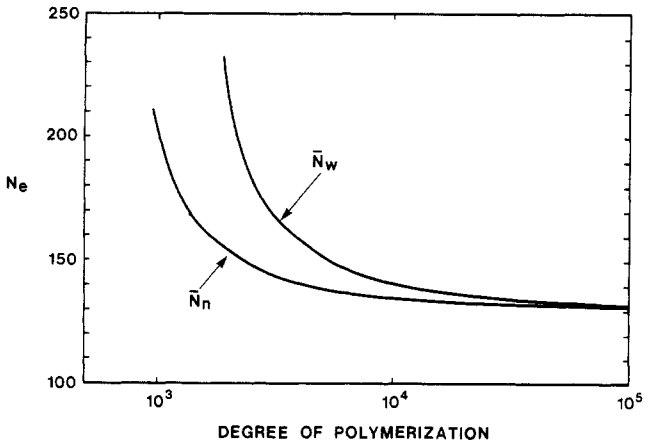

Figure 9. Mean spacing between entanglements, N_e, versus degree of polymerization for a polydisperse system using two common measures of mean chain length with $\tilde{N} = 5$ and $\phi = 1$. For this figure we have varied the polydispersity index, P, according to $P \propto \bar{N}_w^{0.1}$. The curve of N_e plotted versus $\bar{N}_w$ shows a wider range of variation than the corresponding plot versus $\bar{N}_n$.

ber-averaged critical chain length. The weight-averaged critical chain length is then given by $N_{cw} = PN_c$.

Physically, the critical behavior of N_e can be understood again with the help of Figure 2. We have already argued that N_e should increase as the chains are shortened. As the chain lengths approach the critical chain length, the following situation takes place. As we enlarge the spherical volumes to incorporate more nontail segments, in order to compensate for the new tail segments that chain cutting has produced, some nontail segments will have their tails enclosed by the expanded spheres. This in turn will require a further enlargement of the spherical volume. This thought experiment rapidly leads one to the situation where the process becomes self defeating; i.e., the spheres that enclose the complete test chain contain fewer than $\tilde{N}$ nontail segments of other polymers, resulting in a geometrical transition.

The transition region can be analyzed as follows. Consider the function $f(\tilde{N},N_e,N)$ defined by

$$f(\tilde{N},N_e,N) = \tilde{N} + 1 - \frac{\pi\phi}{6}N_e^{1/2}(1 - N_e/N) \quad (22)$$

For every value of $\tilde{N}$ and N, the corresponding value of N_e is the one that satisfies

$$f(\tilde{N},N_e,N) = 0 \quad (23)$$

In Figure 10 we plot $f(\tilde{N},N_e,N)$ as a function of N_e, for several values of N and a fixed value of $\tilde{N} = 4.0$ and $\phi = 1$. Each curve has a minimum and either zero, one, or two intersections with the $f = 0$ axis. The curve with no intersections corresponds to a value of $N < N_c$; i.e., there are no physical solutions. The curve with one intersection is at $N = N_c$. The curve with two intersections is for a value of $N > N_c$. In this situation, we choose the lower value of the two roots, in order that we approach the asymptotic value in a continuous fashion. To determine the value of N_c, we find the value of N_e that simultaneously is a zero of eq 22 and gives a minimum value. Differentiating eq 22 with respect to N_e, we find the minimum is at

$$N_c = 3N_e(N_c) \quad (24)$$

Substituting $N_e = N_c/3$ into eq 22, we then find

$$N_c = \frac{27}{4}\left(\frac{6(\tilde{N} + 1)}{\pi\phi}\right)^2 = \frac{27}{4}N_e(\infty) \quad (25)$$

$$N_c = 3^5[(\tilde{N} + 1)\mu_m/\pi\rho C_\infty^{3/2}l^3]^2 \quad (26)$$

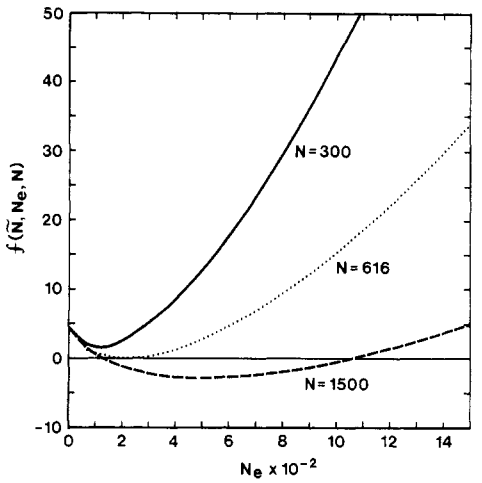

Figure 10. Plots of $f(\tilde{N},N_e) = \tilde{N} + 1 - \pi\phi N_e^{1/2}(1 - N_e/N)/6$ versus N_e for a given choice of N with $\tilde{N} = 4$ and $\phi = 1$. Each curve has a minimum and either zero, one, or two intersections with the $f = 0$ axis. The curve with no intersections corresponds to $N = 300$ which is below N_c ($N_c = 616$ for $\tilde{N} = 4$). The curve with one intersection corresponds to $N = N_c$. The curve with two intersections corresponds to $N = 1500$, which is well above N_c. In this situation, we choose the lower value of the two roots in order that we approach the asymptotic value ($N_e(\infty) = 91$) continuously.

which relates the value of N_c to N_e in the infinite molecular weight limit and consequently to the chain parameters and is a new result.

The sharpness of the transition predicted from eq 17 is partly an artifact of our mean field description of the test segment used in eq 9. The test segment with N_e bonds was assumed to span a distance of $N_e^{1/2}l$, which is the mean distance spanned by the N_e bonds. Since N_e is typically of the order of 10^2–10^3, length fluctuations may play an important role in altering the description of the chain near the transition.[11] Length fluctuations have not been included here in order to retain the simple analytical form of eq 17. However, several of our results are derived in the infinite chain limit and are therefore not affected by this omission.

Despite the approximations we have made, the relationship predicted between N_c and N_e, $N_c/N_e = 6.75$, is in good agreement with experimentally[12] determined ratios of $N_c/N_e \approx 7$ from steady-state compliance measurements but not in particularly good agreement with determinations of $N_c/N_e \approx 2$–3 (although some polymers, such as the methacrylates,[12] yield higher values of about 6) from viscosity data. Graessley has discussed the limitations of determining N_c from viscosity data.[12] The main difficulty, apart from the molecular weight and viscosity determination and the accuracy of interpolation, stems from a need to correct the viscosities to a constant temperature at a constant segmental friction factor.

Equation 26 makes specific predictions on how N_c will change with the various chain parameters. For example, for a fixed skeletal bond length l, N_c varies according to

$$N_c \propto \mu_m^2/C_\infty^3 \quad (27)$$

which agrees with the empirical correlations determined by Privalko.[13] Aharoni[4] has statistically inferred correlations of the form $N_c \propto C_\infty^2$ which appear very different from eq 26, but the two scaling predictions are not entirely inconsistent. For example, for a series of similar polymers where one systematically increases the size of a side group on the chain and therefore increases C_∞, Aharoni's correlations predict that N_c will increase accordingly. Equation 26 will also predict an increase in N_c provided that μ_m^2

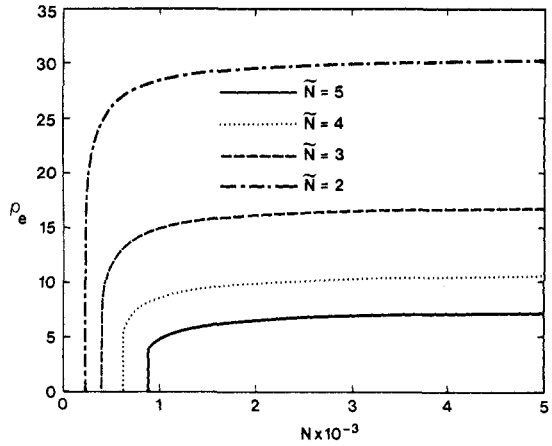

Figure 11. Relative density of entanglements versus degree of polymerization for various values of the coordination number, $\tilde{N}$. Each curve exhibits a discontinuity at $N_c = 3^5(\tilde{N}+1)^2/(\pi\phi)^2$. Below N_c, the mean number of constraining polymers is less than $\tilde{N}$ and the behavior of the test chain is described by classical Rouse dynamics. Polydispersity and length fluctuation can smoothen the transition.

increases more rapidly than C_∞^3, which is often the case. Anomalous points in Aharoni's scatter plots, such as polymeric sulfur ($N_c \sim 3000$, $C_\infty = 1.76$) and cellulose acetate ($N_c \sim 32$, $C_\infty = 23.4$), can be explained by eq 26.

Strong supporting evidence for the geometrical nature of the transition can be found in experimental diffusion and viscosity data,[12] where the onset of entangled behavior occurs at a length N_c, whose value is independent of temperature in agreement with eq 26. Equation 20 leads to a scaling law prediction for the plateau modulus, G_N^0, in concentrated ideal solutions of the form

$$G_N^0 \propto \rho/N_e \propto \phi^{3.0} \tag{28}$$

which is not in especially good agreement with the observed scaling exponents of 2.0–2.3.[12] The discrepency probably stems from assuming that the polymer conformations are Gaussian on the length scale of entanglements. The analysis that follows, for good solvents, leads to an exponent of 2.25, which is in better agreement with the observed exponents.

The values of N_e can be used to calculate the density of entanglements $\rho_e \equiv \rho_m/N_e$. In Figure 11, we plot ρ_e versus N for several values of $\tilde{N}$ and with $\phi = 1$. The density of entanglements exhibits a sharp first-order transition at N_c.

The discussions thus far have focused on polymer melts and concentrated ideal solutions. The same approach can be applied to polymers in good solvents. In a good solvent,[14] the mean blob diameter enclosing N_e segments of the polymer is proportional to $N_e^{3/5}$. Equation 17 then becomes

$$\tilde{N} + 1 = C_1\phi N_e^{4/5}(1 - N_e/N) \tag{29}$$

where C_1 is a certain numerical factor. Analyzing this equation in the same fashion as eq 22 we find in the large N limit that N_e approaches a constant value

$$\lim_{N\to\infty} N_e = [(\tilde{N}+1)/C_1\phi]^{5/4} \tag{30a}$$

$$\lim_{N\to\infty} N_e \propto \phi^{-5/4} \tag{30b}$$

and the lower critical value for entanglements occurs when N is

$$N_c = \frac{9}{4}\left(\frac{9}{5}\right)^{5/4} N_e(\infty) \tag{31a}$$

$$N_c \propto \phi^{-5/4} \tag{31b}$$

which is fundamentally different from eq 25 for ideal solvents. Equation 30, therefore, predicts that the plateau modulus for polymer in good solvents scales with the polymer density according to $G_N^0 \propto \phi^{2.25}$.

Equation 29 also predicted that the concentration threshold ϕ^* for the presence of entanglements, for a chain length N, scales according to

$$\phi^* \propto N^{-4/5} \tag{32}$$

which is the same scaling law as the overlap threshold predicted by de Gennes.[14] In fact, our "blob" analysis can be used to determine the overlap threshold by chosing a low value of $\tilde{N}$ to correspond to an overlap criterion rather than an entanglement criterion.

Equation 17 provides a method for computing N_e as a function of N and for specifying a value of N_c. While our procedure utilizes a static description of the polymer configurations, around a test chain, the connection we have made between $\tilde{N}$ and N_e implicitly contains assumptions about the dynamics. For example, we have excluded neighboring tail segments in the calculation of $\tilde{N}$. While a tail segment may be involved in forming an entanglement with our test chain, it is not expected to be a long-lived entanglement as compared to a nontail segment. The range of N values, for which N_e varies, is the same as the range in which the constraint release process[20] is believed to contribute to deviations from the reptation theory. Although we have not included a constraint release mechanism in this section, our theory of entanglements leads to a similar "dilation" of the tube for entangled chains with N just above N_c.

It is interesting to note that eq 17 predicts that, under the simulation conditions selected by Kolinski et al.,[10] $\phi = 0.5$ and $N = 800$, the system is at best weakly entangled if not unentangled. This may account for the absence of a "tube" image in their Monte Carlo data.

3. Dynamical Theory

The influence of lateral constraints on polymer dynamics, in a melt or concentrated ideal solution, can be investigated with the GRM developed originally for semidilute polymer solutions[15] and applied more recently to polymer melts.[16,17] A similar approach has been used recently to describe rubber elasticity.[18]

Like the original Rouse model,[5] the GRM provides a three-dimensional Fourier analysis of the random diffusional motion of the polymer chain in terms of a bead spring friction coefficient. In the GRM, the relaxation time corresponding to the Fourier mode p is given by

$$\tau(p) = [\zeta(p)\tilde{a}^2(p)C(p)N^2l^2]/[3\pi^2k_BTp^2] \tag{33}$$

where $\tilde{a}^2(p)$ is the square of the strain ratio,

$$\tilde{a}^2(p) = \langle|\tilde{\mathbf{r}}(p)|^2\rangle/\langle|\tilde{\mathbf{r}}(p)|^2\rangle_0 \tag{34}$$

$C(p)$ is a generalized characteristic ratio,

$$C(p) = \langle|\tilde{\mathbf{r}}(p)|^2\rangle_0/Nl^2 \tag{35}$$

$\zeta(p)$ is a wavenumber-dependent friction coefficient which will include hydrodynamic interactions, and l is the length of the atomic bond vectors. The averages in eq 34 and 35 are interpreted as follows: $\langle\ \rangle$ represents an average over the real chain configuration and $\langle\ \rangle_0$ represents an average over the unperturbed Gaussian configuration. Equation 33 reduces to the usual Rouse relaxation times in the small p limit where $C(p) \simeq C(0) \equiv CN = \langle\mathbf{R}^2\rangle_0/Nl^2 = C_\infty$ and $\mathbf{R}$ is the end-to-end vector. For simplicity, we will consider a system where $C(p) = 1$.

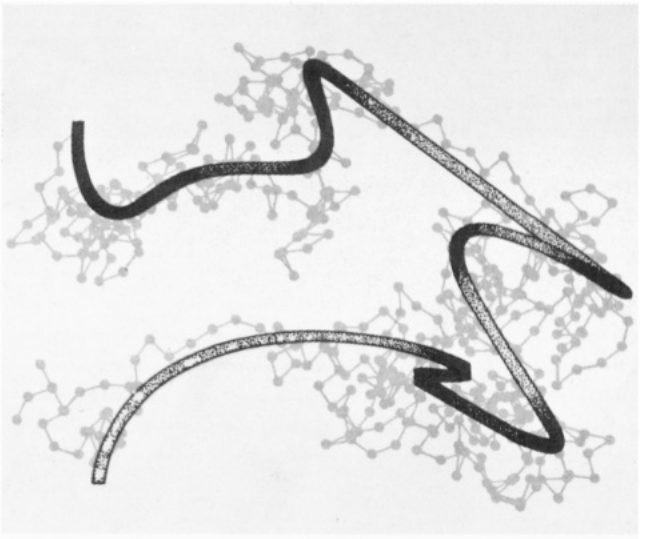

Figure 12. Two-dimensional polymer conformation ($N = 500$) generated by a random flight ($C_\infty = 1$). The smooth curve represents the "tube" axis discussed in the text. The local tangent to the tube axis defines the direction along which unconstrained (longitudinal) diffusion can occur. This curve was generated with the Fourier smoothening method, discussed in section 3, using $\bar{p} = 5$, thus averaging each bond vector over 100 neighboring bond vectors. The transverse directions, at each point along the curve, are those that are normal to the local tangent.

It is now well-known from the pioneering work of Flory[19] that, both in the Θ state and in the melt, polymer conformations are unperturbed and hence $\tilde{a}^2(p) = 1$. For entangled polymers, $\tilde{a}^2(p) = 1$ also holds, but the evolution of the polymers conformation must be anisotropic in accordance with the physical constraints imposed by the surrounding polymers. To see this more clearly, consider the polymer chain depicted in Figure 2. In order to displace the chain through a finite distance roughly along the contour of the chain conformation, one will encounter a certain amount of frictional resistance due to the presence and contacts with other chains. A similar displacement perpendicular to the chain axis will meet with even greater resistance, if the magnitude of the displacement exceeds the spacing between entanglements. Therefore, the presence of entanglements destroys the three-dimensional isotropy of a polymer's diffusional motion and yields nonequivalent longitudinal and transverse modes of motion. We can therefore represent the effect of entanglements in our model by defining wavevector-dependent longitudinal and transverse friction coefficients, $\zeta_l(p)$ and $\zeta_t(p)$, respectively, whose properties are discussed below.

In order to give a formal definition to the longitudinal and transverse directions, we define a "tube" axis with a set of vectors $\hat{\mathbf{r}}(n)$, given by the truncated Fourier series

$$\hat{\mathbf{r}}(n) = \sum_{p=1}^{\bar{p}} \tilde{\mathbf{r}}(p) \sin(\pi pn/N) \tag{36}$$

where $\bar{p}$ is some integer in the range $\bar{p} = 1, 2, 3, ..., N$. The effect of the cutoff, $\bar{p}$, in the previous equation, is to compute a weighted average over $N/\bar{p}$ beads around bead n. In Figure 12 we plot a two-dimensional polymer conformation with 500 Rouse bonds, generated from a random flight, and a Fourier smoothened image of the chain using $\bar{p} = 5$. The Fourier smoothened image represents essentially the same overall conformation of the chain but lacks the small-scale detailed structure of the chain. The tube axis definition above is fundamentally different from the primitive path of Doi and Edwards[3] which is defined by the topological constraints imposed by the neighboring chains. A tube with diameter $(N/\bar{p})^{1/2}l$ drawn along the tube axis will, however, contain the Doi–Edwards primitive path.

While the tube axis is a Fourier smoothened image of a static conformation, if $N/\bar{p}$ is chosen to be the mean spacing between entanglements, N_e, then one can argue that a tube drawn along this axis can also be interpreted as a short-time-averaged or blurred image of the chain. We therefore connect the preceding analysis for N_e with the dynamics by choosing $\bar{p} = N/N_e$.

We now decompose the Langevin equation for each Rouse bond into longitudinal and transverse motions by projecting each bond along the tube axis. The longitudinal components of the bond vectors are therefore

$$\lambda(n) = \mathbf{r}(n)\cdot\hat{\mathbf{r}}(n)/\langle\hat{\mathbf{r}}(n)\cdot\hat{\mathbf{r}}(n)\rangle \tag{37}$$

where the denominator, which is a normalization factor, is

$$\langle\hat{\mathbf{r}}(n)\cdot\hat{\mathbf{r}}(n)\rangle = (4/N^2)\sum_{k=1}^{\bar{p}}\sum_{l=1}^{\bar{p}}\sum_{n'=1}^{N}\sum_{n''=1}^{N}\langle\mathbf{r}(n')\cdot\mathbf{r}(n'')\rangle \times \sin(\pi kn'/N)\sin(\pi kn/N)\sin(\pi ln''/N)\times \sin(\pi ln/N) \tag{38a}$$

$$\langle\hat{\mathbf{r}}(n)\cdot\hat{\mathbf{r}}(n)\rangle = (2l^2/N)\sum_{k=0}^{\bar{p}}[\sin(\pi kn/N)]^2 \tag{38b}$$

$$\langle\hat{\mathbf{r}}(n)\cdot\hat{\mathbf{r}}(n)\rangle = l^2/N_e - (l^2/N)[\sin(2\pi n/N_e)/(2\tan(\pi n/N)) - \sin^2(\pi n/N_e)] \tag{38c}$$

We have used the statistical independence of Rouse bonds

$$\langle\mathbf{r}(n')\cdot\mathbf{r}(n'')\rangle = l^2\delta_{n',n''} \tag{39}$$

to arrive at eq 38. Apart from the Rouse bonds near the chain ends, eq 38c can be written, to a good approximation, as

$$\langle\hat{\mathbf{r}}(n)\cdot\hat{\mathbf{r}}(n)\rangle \approx l^2/N_e \tag{40}$$

Next we define a set of longitudinal or tube Fourier modes, $\tilde{\lambda}(p)$, as

$$\tilde{\lambda}(p) = 2^{1/2}\sum_{n=1}^{N}\lambda(n)\sin(\pi pn/N) \tag{41}$$

The relaxation times of these tube modes, or equivalently the polymer longitudinal diffusional modes, are now given by

$$\tau_l(p) = [\langle\tilde{\lambda}^2(p)\rangle N\zeta_l(p)]/[3\pi^2k_BTp^2] \tag{42}$$

where $\langle\tilde{\lambda}^2(p)\rangle/Nl^2$ is the square of the strain ratio computed *along* the tube axis and is given by

$$\langle\tilde{\lambda}^2(p)\rangle = (8N_el^2/N^2)\times \sum_{n=0}^{N}\sum_{n'=0}^{N}\sum_{k=0}^{\bar{p}}\sum_{m=0}^{N}\sum_{m'=0}^{N}\sum_{l=0}^{\bar{p}}\langle\mathbf{r}(n)\cdot\mathbf{r}(n')\mathbf{r}(m)\cdot\mathbf{r}(m')\rangle \times \sin(\pi kn'/N)\sin(\pi kn/N)\sin(\pi lm'/N)\times \sin(\pi lm/N)\sin(\pi pn/N)\sin(\pi pm/N) \tag{43}$$

The four-point correlation function $\langle\mathbf{r}(n)\cdot\mathbf{r}(n')\mathbf{r}(m)\cdot\mathbf{r}(m')\rangle$ can be factorized, without approximation, as follows:

$$\langle\mathbf{r}(n)\cdot\mathbf{r}(n')\mathbf{r}(m)\cdot\mathbf{r}(m')\rangle = \begin{cases} l^4 & n = n',\ m = m' \\ l^4/3 & n = m,\ n' = m'\ (n \neq n') \\ l^4/3 & n = m',\ m = n'\ (n \neq m) \\ 0 & \text{otherwise} \end{cases} \tag{44}$$

Substituting this into the expression for $\langle\tilde{\lambda}^2(p)\rangle$, we then obtain

$$\langle \tilde{\lambda}^2(p) \rangle = (8l^2N_e/N^2) \times \left[\sum_{n=1}^{N} \sum_{k=1}^{\bar{p}} \sin^2(\pi kn/N) \sin(\pi pn/N) \right]^2 + (4l^2N_e/3N) \sum_{n=1}^{N} \sum_{k=1}^{\bar{p}} \sin^2(\pi kn/N) \sin^2(\pi pn/N) + (8l^2N_e/3N^2) \sum_{n=1}^{N} \sum_{m=1}^{N} \sum_{k=1}^{\bar{p}} \sum_{l=1}^{\bar{p}} (\sin(\pi kn/N) \times \sin(\pi km/N) \sin(\pi ln/N) \sin(\pi lm/N) \times \sin(\pi pn/N) \sin(\pi pm/N)) - (16l^2N_e/N^2) \sum_{n=1}^{N} \sum_{k=1}^{\bar{p}} \sum_{l=1}^{\bar{p}} [\sin(\pi kn/N) \times \sin(\pi ln/N) \sin(\pi pn/N)]^2 \equiv T_1 + T_2 + T_3 + T_4 \quad (45)$$

where the fourth term corrects for overcounting the terms with $n = n' = m = m'$ in the second and third terms. The evaluation of $\langle \tilde{\lambda}^2(p) \rangle$ can be simplified by ordering the various terms according to their scaling relation with respect to the chain length, N, and the wavenumber cutoff, $\bar{p}$. The result of such a classification is

$$T_1 \sim O(\bar{p})O(N^2)$$
$$T_2 \sim O(N)$$
$$T_3 \sim O(N)$$
$$T_4 \sim O(\bar{p})O(N)$$

Since the value of $\bar{p}/N$ is bounded between the values of 0 and 1, to leading order in N (i.e., to order N^2), we have

$$\langle \tilde{\lambda}^2(p) \rangle \approx T_1 = (8l^2N_e/N^2)[\sum_{n=1}^{N} \sum_{k=1}^{\bar{p}} \sin^2(\pi kn/N) \sin(\pi pn/N)]^2 \quad (46)$$

which to order N^2 is well approximated by

$$\langle \tilde{\lambda}^2(p) \rangle \approx \begin{cases} 2l^2/N_e \cot^2(\pi p/2N) & \text{odd } p \\ 0 & \text{even } p \end{cases} \quad (47)$$

For small odd values of p, the previous equation yields the scaling law

$$\langle \tilde{\lambda}^2(p) \rangle \propto N^2/(p^2N_e) \quad (48)$$

The longitudinal mode relaxation times are then computed by substituting eq 47 into eq 42:

$$\tau_l(p) = \begin{cases} 2l^2\zeta_l(p)N/(3\pi^2p^2N_ek_BT) \cot^2(\pi p/2N) & \text{odd } p \\ 0 & \text{even } p \end{cases} \quad (49a)$$

$$\tau_l(p) \propto (\zeta_l(p)N^3/p^4N_e) \quad (49b)$$

The transverse relaxation terms can be obtained in a similar fashion. For wavenumbers $p \geq \bar{p}$, the diffusional motion is not hindered by entanglements, and therefore for motions on these length scales, we have

$$\tau_t(p) = [\zeta_t(p)N^2l^2]/[3\pi^2k_BTp^2] \qquad p \geq \bar{p} \quad (50)$$

For wavenumbers $p < \bar{p}$, the transverse translational diffusion of the test chain *is* hindered by the entangling chains. In the framework of the Rouse theory, the interactions with other chains is purely frictional, since there is no elastic restoring force associated with inter-chain interactions, and we will represent the effect of hindered lateral diffusion by

$$\zeta_l(p) = \zeta_0 \qquad p = 1, 2, ..., N$$
$$\zeta_t(p) = \begin{cases} \zeta_0 & p = \bar{p}, \bar{p}+1, ..., N \\ \infty & p = 1, 2, ..., \bar{p}-1 \end{cases} \quad (51)$$

The effect of a very large, or in the present model infinite, transverse friction coefficient is to retard the lateral diffusion over length scales larger than the mean spacing between entanglements. With the present model for $\zeta_t(p)$, we can apply eq 50 for all p. Additional nonreptative processes, such as the release of constraints,[20] can lead to transverse diffusion for $p < \bar{p}$. These effects can be included in this model by modifying eq 51.

4. Relaxation Spectrum

We now combine the results of sections 2 and 3 to compute the relaxation spectrum for melts of linear polymers as a function of the degree of polymerization. Of particular interest is the longest relaxation time, τ^*, which determines the long time behavior of the melt. These relaxation times determine many of the rheological and transport properties of the melt, which are the subject of a future article.[21]

In section 3, we have shown that there is a fundamental difference between the three-dimensional isotropic diffusion in an unentangled melt ($N < N_c$) and the quasi-one-dimensional motion that occurs in an entangled melt ($N \geq N_c$). Section 2 provides a prescription for computing N_c, as well as N_e, for polymer lengths $N \geq N_c$. The value of N_c is essentially determined by one parameter, $\tilde{N}$, and one characteristic property of the melt, ϕ, which contains information on the density of the melt, the monomer composition, and the characteristic ratio.

The relaxation spectrum in the unentangled regime is given by

$$\tau(p) = [\zeta_0N^2l^2]/[3\pi^2k_BTp^2] \qquad N \leq N_c \quad (52)$$

For lengths $N > N_c$, we have according to eq 49 and 51

$$\tau(p) = \begin{cases} [2l^2\zeta_0N]/[3\pi^2N_e(N)p^2k_BT] \cot^2(\pi p/2N) & N \geq N_c, \; p \leq \bar{p} \\ [\zeta_0l^2N^2]/[3\pi^2k_BTp^2] & N \geq N_c, \; p > \bar{p} \end{cases} \quad (53)$$

where $N_e(N)$ is given by the solution of

$$\tilde{N} + 1 = \pi\phi N_e^{1/2}(N)(1 - N_e(N)/N)/6 \quad (54)$$

The first part of eq 53 describes the diffusional relaxation over length scales longer than the mean spacing between entanglements that must occur along the curvilinear coordinate of the tube axis defined in section 3. The second part of eq 53 describes diffusional relaxation over shorter length scales, which can be either transverse or longitudinal with respect to the tube axis.

The form of the relaxation spectrum that we predict for the entangled regime is fundamentally different than the de Gennes[2] and Doi–Edwards[3] theories where

$$\tau_{rep}(p) = [\zeta_0l^2N^3]/[\pi^2N_ek_BTp^2] \quad (55)$$

Apart from a numerical factor of $8/3\pi^2$, the major difference between eq 53 and eq 55 is an additional factor of p^2 in the denominator of eq 53. The two theories do however give the same expression for the zero frequency shear viscosity, η_0, apart from a factor of 1/3. From the reptation theory[6] we have

$$\eta_0^{rep} \propto \int_0^\infty dt \; \psi_{rep}(t) \quad (56)$$

where

$$\psi_{rep}(t) = \sum_{p=1,3,5,etc.} 8/(p^2\pi^2)e^{-t/\tau_{rep}(p)} \quad (57)$$

and therefore

$$\eta_0^{rep} \propto \sum_{p=1,3,5,etc.} 8\tau_{rep}(p)/(p^2\pi^2) \quad (58)$$

For the GRM, $\psi_{GRM}(t)$ is[6]

$$\psi_{GRM}(t) = \sum_{p=1,2,3,etc.} e^{-t/\tau_{GRM}(p)} \quad (59)$$

and therefore

$$\eta_0^{GRM} \propto \sum_{p=1,3,5,etc.} \tau_1(p) = (1/3)\eta_0^{rep} \quad (60)$$

The even values of p are excluded from the summation above, making use of eq 49.

The longest relaxation times are therefore given by

$$\tau^* = \begin{cases} [\zeta_0 l^2 N^2]/[3\pi^2 k_B T] & N < N_c \\ [8\zeta_0 l^2 N^3]/[3\pi^4 N_e k_B T] & N \geq N_c \end{cases} \quad (61)$$

and are plotted as a function of N for several values of $\tilde{N}$ in Figure 13. The most striking feature of this plot is the sharp discontinuity in τ^* at the transition point, N_c. The discontinuity is partly a consequence of the mean field description of the chain used in section 2 and, in particular, the absence of length fluctuations. The discontinuity here is smaller, by a factor of about 3.7, than the discontinuity between the reptation and Rouse theories at N_c.

The plot of τ^* versus N, for $N \gtrsim N_c$, deviates from the usual reptation scaling law, $\tau^* \propto N^3$, through the small N dependence of $N_e(N)$. This N dependence disappears in the long polymer limit but yields an *effective* scaling law of the form

$$\tau^* \propto N^{3+\gamma(N)} \quad (62)$$

for N just above N_c, with the coefficient $\gamma(N)$ varying from a value of about 1/2 for $N \gtrsim N_c$ and tending to zero for larger N. The effective scaling exponent, $\gamma(N)$, is plotted versus degree of polymerization for $\tilde{N} = 5$ and $\phi = 1$ in Figure 14. This plot shows that the value of $\gamma(N)$ and the range over which $\gamma(N)$ varies can be influenced by polymer polydispersity if the polydispersity index is dependent on $\tilde{N}_w$. The principal result here is that the chain length dependence of τ^* is not of the simple algebraic form derived in the reptation theory[2,3] but may be expressed in that form over a range of values of chain length.

It is interesting to note that in reptation-like theories, the self-diffusion coefficient and zero shear viscosity[14] depend differently on the parameter N_e:

$$\eta_0 \propto N^3/N_e^2 \quad (63)$$

$$D_{self} \propto N_e/N^2 \quad (64)$$

Consequently, the deviations from their respective power laws, $D_{self} \propto N^{-(2+\gamma)}$ and $\eta^0 \propto N^{(3+\delta)}$, are related in the present theory by $\delta = 2\gamma$. This result is consistent with diffusion experiments where the exponent γ is usually in the range of 0–0.2.[22-25] In mutual diffusion studies, where a tracer species diffuses in a fixed high molecular weight matrix, *the parameter N_e is constant*. Consequently, no deviations from $D_{mut} \propto N^{-2}$ are predicted, which is also consistent with recent experiments.[22]

5. Summary and Conclusions

The purpose of this paper is twofold. First, we have presented a new description of entanglements in dense polymer systems by making an ansatz connecting lateral constraints with the presence of a certain number of neighboring nontail segments. This theory introduces a new parameter, $\tilde{N}$, in the discussion of the entangled state, which replaces the phenomenological parameter, N_e, in the original reptation theory.[2,3] Our approach yields *predictions* for the values of N_e and N_c, as a function of various chain parameters, polydispersity, and concentration, for both melts and concentrated solutions.

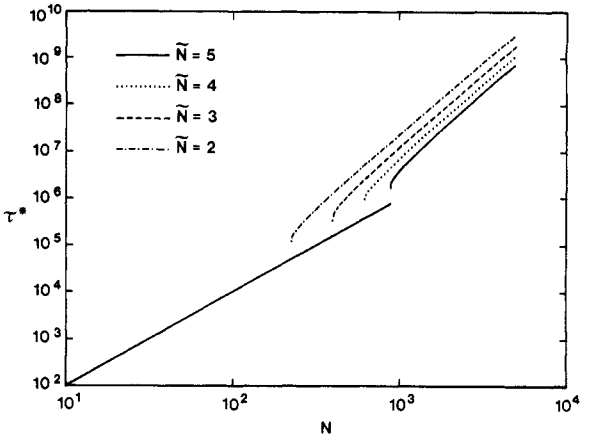

Figure 13. Longest relaxation time versus number-averaged degree of polymerization for several values of $\tilde{N}$. For N below each curve's respective value of $N_c = 3^5(\tilde{N}+1)^2/(\pi\phi)^2$, the relaxation dynamics are isotropic in three dimensions and $\tau^* \propto N^2$ according to the Rouse theory. Above N_c, the relaxation times approach the reptation theory results with $\tau^* \propto N^3$. The transition region is characterized by deviations from the reptation theory and can be affected by polydispersity as discussed in the text.

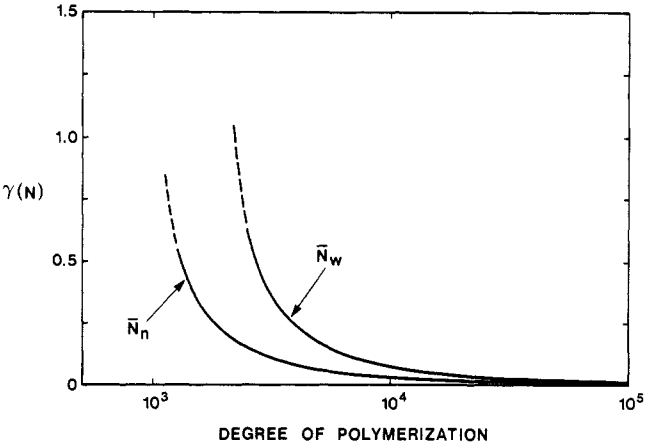

Figure 14. Scaling correction $\gamma(N)$ for the relaxation times, $\tau \propto N^{3+\gamma(N)}$, versus degree of polymerization using two common measures of mean chain length. This calculation includes the polydispersity effects used in Figure 9. The scaling correction $\delta(N)$ for the zero frequency shear viscosity, $\eta_0 \propto N^{3+\delta(N)}$, is $\delta(N) = 2\gamma(N)$. The figure illustrates that the range over which $\delta(N)$ varies is influenced by polydispersity. Length fluctuations are also expected to broaden this range.

Second, we have outlined a prescription for applying a Rouse description of polymer dynamics to the entangled state. A tube axis was defined by Fourier smoothening the polymer conformation using a smoothing length scale determined by the mean entanglement spacing. The dynamics of the Fourier smoothened image, which correspond to the dynamics of the polymer's collective modes, was then calculated by imposing a wavenumber-dependent friction coefficient to account for entanglement effects. The principle result here was the relaxation spectrum for the polymer conformation as a function of degree of polymerization.

For polymer lengths $N < N_c$, our theory corresponds to the original Rouse theory. For very long polymers, our predictions for the relaxation spectrum are different from the reptation theory. Our predictions for the zero shear viscosity, however, agree with the reptation theory. For intermediate polymer lengths, $N \gtrsim N_c$, the relaxation

spectrum predicted deviates from the reptation theory results, yielding an effective scaling exponent, with N, larger than 3. Our theory predicts that the deviations from the N^3 power law for the viscosity and the deviations from the N^{-2} power law for the self-diffusion coefficient are related but are not of the same magnitude. These deviations were shown to be sensitive to polydispersity.

Several issues still remain to be addressed. We have conjectured that the entangled state of polymers can be described by a dimensionless parameter $\tilde{N}$ which may be universal. We have not however indicated what the value of $\tilde{N}$ is, apart from a plausible range of values (3–6). The search for $\tilde{N}$ may be approached from several fronts including computer simulations, topological theories, and an analysis of the vast amount of experimental data. One critical issue still outstanding is the long-chain limit. Our description of entanglements predicts that the reptation theory results are valid in this limit. This point has not however been clarified in the experimental literature. The theory that we have presented is a first level or mean field theory, and we expect that improvement, such as the addition of fluctuation phenomena and clarification of the relationship between this theory and the constraint release mechanism, should yield more insight into this problem. We will address some of these issues in a future article.[21]

Acknowledgment. The authors would like to thank L. M. Marks for many stimulating discussions and his assistance in the computer simulations. T. A. Kavassalis would like to thank the National Sciences and Engineering Research Council of Canada for financial support in the form of an Industrial Research Fellowship.

Note Added in Proof. The analysis of entanglement scaling for polymers in semidilute solution, in section 2, is somewhat flawed. The results, however, are qualitatively correct and a more careful derivation will be published in a future article.

References and Notes

(1) Ferry, J. D. *Viscoelastic Properties of Polymers*; Wiley: New York, 1980 and references contained within.
(2) de Gennes, P.-G. *J. Chem. Phys.* **1971**, *55*, 572.
(3) Doi, M.; Edwards, S. F. *J. Chem. Soc., Faraday Trans. 2* **1978**, *74*, 1789, 1802, 1818.
(4) Aharoni, S. H. *Macromolecules* **1983**, *16*, 1722; **1986**, *19*, 426.
(5) Rouse, P. E. *J. Chem. Phys.* **1953**, *21*, 1272.
(6) Doi, M.; Edwards, S. F. *The Theory of Polymer Dynamics*; Oxford University Press: Oxford, 1986.
(7) Hess, W. *Macromolecules* **1987**, *20*, 2587.
(8) Green, M. S. *J. Chem. Phys.* **1952**, *20*, 1281.
(9) Kubo, R. *Lectures in Theoretical Physics*; Wiley: New York, 1958; Vol. 1, p 120.
(10) Kolinski, A.; Skolnick, J.; Yaris, R. *J. Chem. Phys.* **1987**, *86*, 1567.
(11) Doi, M. *J. Polym. Sci. Lett.* **1981**, *19*, 265.
(12) Graessley, W. W. *Adv. Polym. Sci.* **1974**, *16*, 1.
(13) Privalko, V. P. *Macromolecules* **1980**, *13*, 370.
(14) de Gennes, P. G. *Scaling Concepts in Polymer Physics*; Cornell University Press: Ithaca, 1979.
(15) Allegra, G.; Ganazzoli, F. *J. Chem. Phys.* **1985**, *83*, 397.
(16) Noolandi, J.; Slater, G. W.; Allegra, G. *Makromol. Chem. Rapid Commun.* **1987**, *8*, 51.
(17) Kavassalis, T. A.; Noolandi, J. *Phys. Rev. Lett.* **1987**, *59*, 2674.
(18) Edwards, S. F.; Vilgis, Th. *Polymer* **1986**, *27*, 483.
(19) Flory, P. J. *J. Chem. Phys.* **1949**, *17*, 303.
(20) Graessley, W. W. *Adv. Polym. Sci.* **1982**, *47*, 67.
(21) Kavassalis, T. A.; Noolandi, J., unpublished results, 1988.
(22) Antonietti, M.; Coutandin, J.; Sillescu, H. *Macromolecules* **1986**, *19*, 793.
(23) Green, P. F.; Palmstrøm, C. J.; Mayer, J. W.; Kramer, E. J. *Macromolecules* **1985**, *18*, 501.
(24) Bartels, C. R.; Christ, B.; Graessley, W. W. *Macromolecules* **1984**, *17*, 2702.
(25) Smith, B. A.; Samulski, E. T.; Yu, L. P.; Winnik, M. A. *Macromolecules* **1985**, *18*, 1901.